

Nonequilibrium phonon distribution in current-driven nanostructures

Guanxiong Chen¹, Ryan Freeman¹, Andrei Zholud¹, and Sergei Urazhdin¹

¹*Department of Physics, Emory University, Atlanta, GA, USA.*

We experimentally demonstrate that electric current applied at cryogenic temperatures to thin-film metallic wires on thermally conducting substrates produces a non-equilibrium phonon distribution. The latter is manifested by the piecewise-linear dependence of resistance on current, inconsistent with Joule heating. Analysis shows that this dependence contains information about the rate of phonon relaxation, and the characteristics of electron-phonon scattering. Our results open a new route for the characterization of electron-phonon interaction at nanoscale, and for the optimization of thermal properties of electronic nanodevices.

Downscaling of modern electronic devices and circuits places ever increasing demands on the efficiency of heat dissipation under increasingly non-equilibrium conditions. Electrical energy is dissipated in materials carrying electric current at a rate $w = \rho J^2$ per unit volume, where J is the current density and ρ is the material's resistivity. In the Joule heating approximation, this energy is assumed to be converted into heat - a quasi-equilibrium distribution of phonons and electrons characterized by an elevated local temperature T^* [1]. Their subsequent diffusion, usually described by the Fourier's equation, dissipates the generated thermal energy away from the heated region [2]. Since most materials exhibit a significant variation of resistivity with temperature, its current-dependence is commonly utilized for the characterization of Joule heating in nanostructures [3, 4].

Recent studies have shown that the quasi-equilibrium picture of Joule heating and diffusive heat dissipation starts to break down at nanoscale [5, 6], because electrons and/or phonons can escape from the system before they thermalize. For instance, if electrons can quickly escape and are sufficiently weakly coupled to phonons, their effective temperature can be significantly lower than that of phonons, resulting in complex nonlocal energy transfer processes between the two subsystems [7–12]. Electrons and/or phonons may also form a nonequilibrium distribution within the respective subsystem, which cannot be characterized by an effective temperature [13–15]. Significant progress has been recently achieved in the understanding of non-equilibrium states of electrons and phonons at nanoscale [16–20]. However, a comprehensive microscopic understanding of current-induced thermal energy generation and transport has not yet emerged.

Here, we experimentally demonstrate that at cryogenic temperatures, common nanostructures such as thin-film metallic wires on thermally conducting substrates exhibit a linear variation of resistance with current, inconsistent with Joule heating. Analysis shows that the observed linear dependence is caused by the substantially non-equilibrium phonon distribution facilitated by the fast phonon escape from the system. At higher temperatures and small currents, the linear dependence becomes smoothed-out, but signatures of nonequilibrium phonon

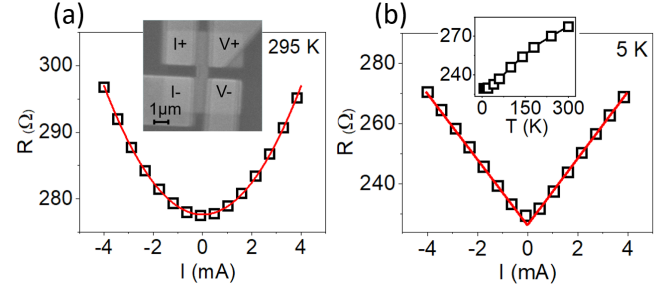


Figure 1. (Color online). Resistance vs current for a 1 μm -long, 500 nm-wide Pt(5) wire, at room temperature $T = 295$ K (a) and at $T = 5$ K (b). Curves are best fits to the data with a quadratic function (a), and with the piecewise-linear function $R(I) = R(0) + \alpha|I|$ (b). Insets: SEM image of the sample (a) and the dependence of resistance on temperature at $I = 0$ (b).

distribution persist at temperatures as high as 200 K. Our results provide insight into the nonequilibrium electron and phonon dynamics at nanoscale, and suggest new approaches to the characterization of electron-phonon interaction and the optimization of thermal management in electronic nanodevices.

Below, we discuss the results mainly for thin-film Pt wires on undoped Si substrates. Similar wires are extensively utilized for spin current generation in spin-orbitronic devices that rely on the spin Hall effect exhibited by Pt [21–25], as well as microscale heaters and thermometers [26]. The generality of the observed behaviors was confirmed by additional measurements of Au wires, as briefly discussed below, Pt wires on different substrates, and metallic nanocontacts [27]. The wires were fabricated by a combination of e-beam lithography and high-vacuum sputtering. To ensure consistent thermal contact between the wires and the substrate, native surface oxide was removed from the Si surface by HF etching immediately prior to the Pt wire deposition. The wires were contacted by Cu(150) electrodes for four-probe resistance measurements [inset in Fig. 1(a)]. Thicknesses are given in nanometers. Electrical resistance was measured using the standard lock-in technique, with ac current $I_{ac} = 10$ μA rms superimposed with the dc current

I of up to 4 mA.

Figure 1 shows representative resistance vs current curves for a 1 μm -long and 500 nm-wide Pt(5) wire. At the experimental temperature $T = 295$ K, the resistance $R(I)$ follows a quadratic dependence on current [Fig. 1(a)]. This result is consistent with Joule heating. Indeed, electrical energy is dissipated in the wire at a rate $W = RI^2$. Since the rate of thermal energy dissipation from the wire is proportional to its temperature increase, one can expect that the temperature of the wire follows a quadratic dependence on current $T^* \approx T_0 + CI^2$. The resistance linearly depends on temperature close to $T = 295$ K [inset in Fig. 1(b)]. Thus, $R(I)$ is expected to follow a quadratic dependence, in agreement with our data.

At $T = 5$ K, the dependence $R(I)$ is well described by the piecewise-linear function $R(I) = R_0 + \alpha|I|$, where α is a constant [Fig. 1(b)]. This dependence cannot be explained by Joule heating. In particular, numerical simulations confirm that for Joule heating, the dependence of the Pt wire temperature on current $T^*(I)$ should be quadratic even at cryogenic temperatures [27]. The resistance of Pt is almost independent of temperature up to 20 K, due to the dominance of impurity/surface scattering, and starts to increase approximately linearly with T at higher temperatures [inset in Fig. 1(b)]. As a consequence, Joule heating should not affect R for currents up to 1.8 mA, and lead to an approximately quadratic dependence $R(I)$ for larger currents [27]. The discrepancy with the observed behaviors indicates that the assumption of quasi-equilibrium distribution underlying the Joule heating picture is not valid. Indeed, analysis presented below shows that the linear $R(I)$ dependence is associated with non-thermalized distribution of phonons generated by the current, which cannot be described by a temperature.

As the temperature is increased from 5 K, the linear dependence remains evident at large currents, but the zero-current singularity becomes increasingly smoothed-out [Fig. 2(a)]. At $T \leq 200$ K, the dependence is well approximated by the function $R(I) = R(0) + \alpha|I|$ convolved with the Gaussian [curves in Fig. 2(a)]. At $T > 200$ K, the width ΔI of the Gaussian becomes larger than the range of the dc current scan, resulting in a significant uncertainty of the fitting. Nevertheless, these data suggest that a non-equilibrium current-driven phonon distribution, not described by Joule heating, can be formed at sufficiently large bias even in the ambient temperature range.

The Gaussian width ΔI follows a linear dependence at $T > 20$ K, extrapolating to $\Delta I = 0$ at $T = 0$ [right scale in Fig. 2(b)]. This indicates that the observed broadening of $R(I)$ originates from the thermally induced spectral broadening of the electron distribution, whose width is proportional to temperature. Thus, the broadening of $R(I)$ can be interpreted in terms of the competition

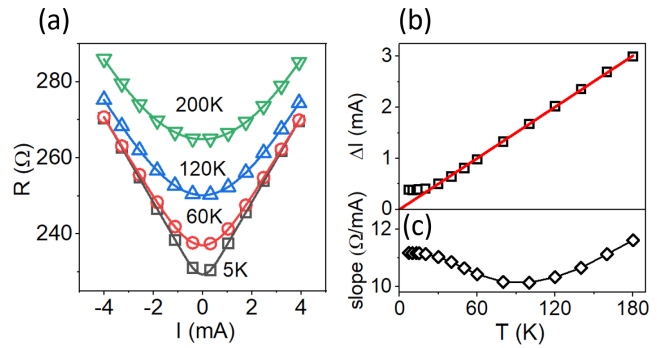


Figure 2. (Color online). (a) Symbols: R vs I for the same sample as in Fig. 1, at the labeled values of T . Curves: best fits with the piecewise-linear function $R(I) = R_0 + \alpha|I|$ convolved with the Gaussian $g(I) = \frac{1}{\sqrt{2\pi}\Delta I} e^{-I^2/2\Delta I^2}$. Some of the data points are omitted for clarity, but fitting was performed for the entire data set. (b),(c) Parameters extracted from the data fitting: the Gaussian width ΔI (b) and the slope of the linear dependence (c). The line in (b) is the best linear fit of the data for $T > 20$ K.

between the thermal energy $k_B T$ of electrons, and the average energy acquired by electrons between scattering events due to the electric field in the Pt wire. The broadening saturates at $T < 20$ K, suggesting the existence of an additional non-thermal broadening effect. Indeed, at small bias and low temperatures, the energy (and thus the momentum) of phonons generated by current is small, resulting in a reduced contribution of the generated phonons to electron momentum scattering, and thus resistance.

The slope of the linear dependence slightly varies with temperature, decreasing with increasing temperatures up to 90 K, and then increasing at higher temperatures [Fig. 2(c)]. These variations can be explained by the temperature dependence of phonon relaxation rate, which is dominated by the dissipation into the substrate, as shown below. Indeed, the observed variations of the slope are correlated with the temperature dependence of thermal conductivity of Si [27]. However, there is no quantitative correspondence between the two quantities, suggesting that phonon escape into the substrate may not be adequately described by the diffusive approximation of heat transport. This conclusion is supported by the analysis of phonon transport presented below.

Non-equilibrium phonon distribution in the studied Pt wires, manifested by the linear dependence $R(I)$, is likely associated with fast relaxation of phonons due to their efficient escape from the system, before they become thermalized. To elucidate the mechanisms of phonon relaxation, we analyze the effects of the wire geometry. Phonons are expected to dissipate mainly into the thick Cu leads and the substrate. Dissipation into the leads becomes less efficient, per unit Pt volume, with increasing wire length, while dissipation in the substrate should

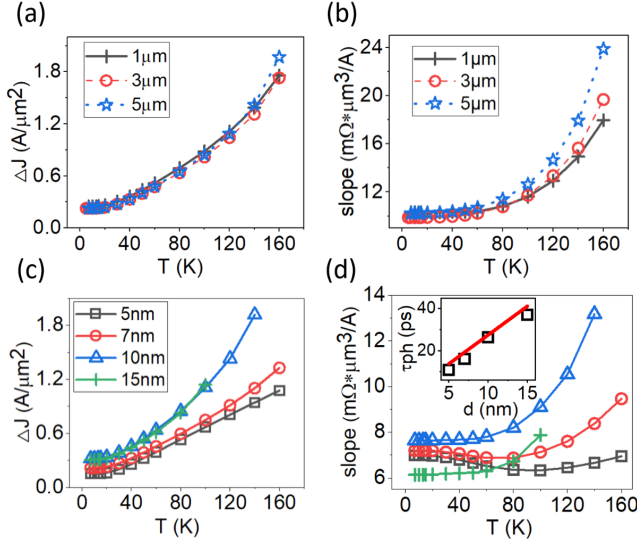


Figure 3. (Color online). Effects of the Pt wire geometry. (a),(b) Temperature dependence of the Gaussian broadening width ΔJ (a) and the linear slope (b) of $\rho(J)$, for the Pt(10) wire lengths of 1 μm , 3 μm , and 5 μm , as labeled. (c),(d) Same as (a), (b), for the 1 μm -long Pt wires with thicknesses 5 nm, 7 nm, 10 nm, and 15 nm, as labeled in (c). Inset in (d): Dependence of the phonon relaxation rate τ_{ph} on the Pt thickness, determined from the data at $T = 5$ K using Eq. (2) (symbols), and calculated based on the acoustic mismatch theory (line).

not be affected by the wire length. The converse is expected, in the diffusive phonon transport regime, for the dependence on the wire thickness.

Figure 3 summarizes the results for different lengths L and thicknesses d of Pt wires. To facilitate direct comparison of different geometries, we analyze the dependence of resistivity $\rho = RA/L$ on the current density $J = I/A$, where A is the cross-section area of the wire. In all cases, we obtained accurate fits of the data by using a piecewise-linear dependence convolved with the Gaussian. For the thickest (15 nm) Pt wire, the analysis is limited to $T \leq 100$ K, because of the large thermal broadening for this thickness.

The thermal broadening ΔJ is independent of the wire length [Fig. 3(a)]. The linear slope of $\rho(J)$ is almost independent of the wire length at temperatures up to about 80 K, and starts to increase with the wire length at higher temperatures. However, the dependence on the wire length remains modest even at $T = 160$ K. Thus, we conclude that at cryogenic temperatures, phonons relax in the studied Pt wires predominantly through the substrate.

In contrast to the effects of the wire length, wire thickness significantly affects the characteristics of $\rho(J)$, Figs. 3(c),(d). The broadening increases by a factor of two when d is increased from 5 nm to 10 nm, and saturates at larger d . For Pt(5), it increases linearly with

temperature $T > 20$ K. This result is consistent with our interpretation of the broadening in terms of the competition between the electron's thermal energy kT and the energy $\propto J$ provided by the electric field between electron scattering events. The observed curving of the dependence $\Delta J(T)$ for larger Pt thickness, especially apparent in Fig. 3(c) for Pt(10) and Pt(15), can be attributed to the larger relative contribution of electron-phonon scattering to the electron mean free path, resulting in the reduction of energy acquired by electrons between the scattering events.

The linear slope of $\rho(J)$ also exhibits a significant dependence on the wire thickness, especially apparent at higher temperatures [Fig. 3(d)]. The slope increases with wire thickness up to 10 nm, and then decreases for Pt(15), in the temperature range up to 100 K where the broadening was sufficiently small to allow a reliable determination of the slope. These nonmonotonic variations can be explained by the competition between the decrease of the phonon generation rate, with increasing Pt thickness, due to the smaller contribution of scattering at the Pt interfaces, and the increase of phonon escape time, as shown by the analysis below [see also inset in Fig. 3(d)].

To interpret the observed behaviors, and to evaluate the material parameters that control the non-equilibrium phonon distribution, we perform kinetic rate analysis of the current-driven phonon population. In the Drude approximation, the electron mean free path is $l_e = \frac{m^* v_F}{n e^2 \rho}$, where v_F and m^* are the Fermi velocity and the effective mass, respectively [28]. In the presence of electric field, the rate of electron scattering per unit volume is $r = \frac{J}{e l_e} = \frac{n e \rho}{v_F m^*} J$. Assuming that one phonon is generated in each scattering event, the rate of phonon generation per unit volume is $\frac{dn_{ph}}{dt}|_{gen} = r$. Relaxation due to the quasi-ballistic phonon escape from Pt [27] can be described by the relaxation time approximation $\frac{dn_{ph}}{dt}|_{rel} = -\frac{n_{ph} - n_0}{\tau_{ph}}$, where n_0 is the phonon population in the absence of current, and τ_{ph} is the relaxation time, which is equal to the phonon escape time due to the rapid phonon escape. In the steady state, $\frac{dn_{ph}}{dt}|_{gen} + \frac{dn_{ph}}{dt}|_{rel} = 0$, or

$$n_{ph} = n_0 + \frac{\tau_{ph} n e \rho}{v_F m^*} J. \quad (1)$$

According to this relation, phonon population depends linearly on current, in the limit of negligible thermalizing phonon-phonon scattering that does not conserve phonon population [27]. Resistivity is then expected to also vary linearly with current, provided that the generated phonons efficiently scatter electrons, i.e. their characteristic momentum is comparable to the Fermi momentum of electrons. These behaviors can be contrasted with Joule heating, which results in a quadratic or even slower dependence $\rho(J)$, as discussed above in the context of Fig. 1. However, the dissipated electric power

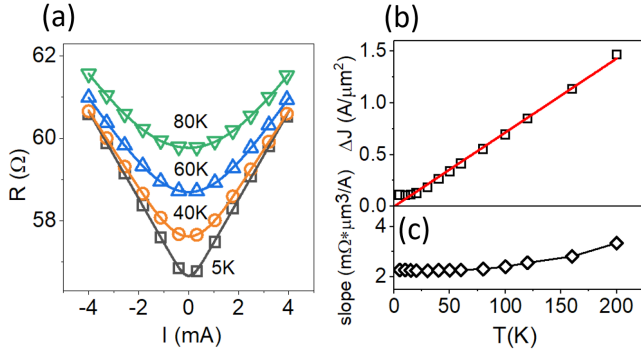


Figure 4. (Color online). (a) Symbols: resistance vs current for a $1\ \mu\text{m}$ -long, $500\ \text{nm}$ -wide Au(5) wire on Si substrate, at the labeled values of temperature. Curves: results of the data fitting using piecewise-linear function $R(I) = R(0) + \alpha|I|$ convolved with the Gaussian. (b),(c) Parameters extracted from the data fitting: the Gaussian width ΔI (b) and the slope of the linear dependence (c). The line in (b) is the best linear fit of the data for $T > 20\ \text{K}$.

$w = \rho J^2$ is the same in both limits. Thus, in contrast to Joule heating, the average energy of the nonequilibrium phonons described by Eq. (1) is proportional to J .

To establish the quantitative relationship between the current dependence of resistance and phonon generation/relaxation characteristics, we use Matthiessen's rule for the electron mean free path in the presence of current-generated phonons, $1/l_e = 1/l_{e,0} + n_{ph}\sigma_{e-ph}$. Here, $l_{e,0}$ is the mean free path in the absence of phonons, and σ_{e-ph} is the average electron-phonon scattering cross-section. Combining with Eq. (1) and neglecting the nonlinear effect of electron-phonon scattering on the phonon population, we obtain

$$\rho(J) = \rho(0)(1 + \tau_{ph}\sigma_{e-ph}J/e). \quad (2)$$

This result demonstrates that the linear slope of the dependence $\rho(J)$ provides direct information about phonon relaxation and electron-phonon scattering. For Pt, we use σ_{e-ph} determined from the temperature dependence of resistivity [27] to calculate the values of τ_{ph} for different Pt wire thicknesses [inset in Fig. 3(d)]. The thickness-dependent values of τ_{ph} , determined from the $T = 5\ \text{K}$ data, are in a remarkable agreement with the acoustic mismatch theory [27]. These results confirm that phonon relaxation in the studied Pt wires is dominated by the fast quasi-ballistic phonon escape into the substrate, which facilitates non-equilibrium current-driven phonon distribution.

We have confirmed the general relevance of the observed behaviors to nanostructures with efficient thermal dissipation, by measurements of current-dependent resistance in Pt wires fabricated on different substrates, as well as metallic nanocontacts [27]. Here, we discuss the results for an Au(5) wire deposited on HF-cleaned un-

doped Si substrate. A Ni(0.5) wetting layer was inserted between Au(5) and the substrate, to improve adhesion and ensure the continuity of the ultrathin Au(5). The geometry of this wire was identical to that of the Pt(5) wire in Figs. 1, 2. At $T = 5\ \text{K}$, the current dependence of resistance is well approximated by the piecewise-linear function [Fig. 4(a)], in agreement with the results for Pt. This dependence becomes increasingly broadened with increasing temperature, with the broadening proportional to temperature at $T > 20\ \text{K}$ [Fig. 4(b)]. The broadening follows a similar dependence to that for Pt(t), scaled by about 0.8. At $T = 5\ \text{K}$, the resistance of the Au(5) wire is 4 times smaller than that of Pt. Meanwhile, the linear slope is almost 3.5 times smaller than for Pt(5). In contrast to Pt(5), the slope for Au(5) monotonically increases with temperature. This dependence is similar to that observed for Pt(10) and Pt(15), but the magnitude of the variations is smaller, closer to Pt(5) and Pt(10).

The differences between the results for Pt and Au can be explained by several factors. First, the estimated electron-phonon scattering cross-section in Au is slightly smaller, $\sigma_{e-ph,Au} = 1.3 \times 10^{-22}\ \text{m}^2$. Based on the measured slope of $R(I)$, we estimate that τ_{ph} in the Au(5) wire is 19 ps at 5 K, almost twice as large as that in Pt(5). In contrast, the phonon escape time calculated from the acoustic mismatch at Au/Si interface is 8 ps, less than half of the experimental relaxation time. We speculate that the discrepancy between the two values originates from the poor wetting by Au of the substrate, resulting in reduced phonon transparency of its interface with Si. Elucidating the relationship between wetting and phonon transparency of interfaces, by measurements such as those presented here, may be important for optimizing the thermal properties of nanoelectronic devices.

To summarize, thin-film metallic wires fabricated on thermally conducting substrates exhibit piecewise-linear dependence $R(I)$ of resistance on current, inconsistent with Joule heating. The linear dependence is observed at sufficiently high currents at temperatures as high as 200 K. This dependence is associated with the nonequilibrium distribution of phonons generated by the electron scattering on impurities and interfaces, which is facilitated by the rapid phonon escape from the system. Analysis indicates that the observed current dependence contains information about the electron-phonon scattering and the phonon relaxation rate.

Our results have broad implications for the optimization of thermal properties of electronic devices and nanostructures. For instance, at high current densities, the linear dependence $R(I)$ associated with the non-equilibrium phonon distribution can fall significantly below the approximately quadratic dependence expected for Joule heating. In this regime, the average energy of phonons generated by current is larger than that of thermal phonons described by Joule heating, but their popu-

lation is smaller than the thermalized population with the same total energy. This regime may be advantageous for the optimization of thermal management in nanoscale devices, for several reasons. First, additional energy dissipation due to electron scattering on the generated phonons can be significantly smaller than in the Joule heating limit, reducing the possibility of thermal runaway [17]. Second, the escape of the generated nonequilibrium phonons from the system can be more efficient than for Joule heating, due to the smaller rates of phonon-phonon scattering. Finally, the generated high-frequency phonons are less likely to contribute to current-induced physical degradation associated with the slow metastable mechanical degrees of freedom.

Current-induced phenomena have been extensively studied in the context of spin Hall effect, in thin Pt films similar to those discussed in our work [4, 21–25]. Our results may warrant re-examination of the Joule heating effects in these experiments. Similarly, low-temperature thermoelectric measurements at nanoscale commonly employ resistive heating of wires similar to those analyzed in our study. As we have shown, such resistive heating can result in strongly nonequilibrium distribution characterized by substantially different phonon density (and its gradients) than inferred from Joule heating. We also note that the nonequilibrium phonon effects discussed above may have contributed to the piecewise-linear current dependence of resistance recently observed at cryogenic temperatures in nanoscale spin valves, and attributed to quantum magnetization fluctuations [29].

This work was supported by the U.S. Department of Energy (DOE), Basic Energy Sciences (BES), under Award # DE-SC2218976.

DEPENDENCE ON THE SUBSTRATE TYPE

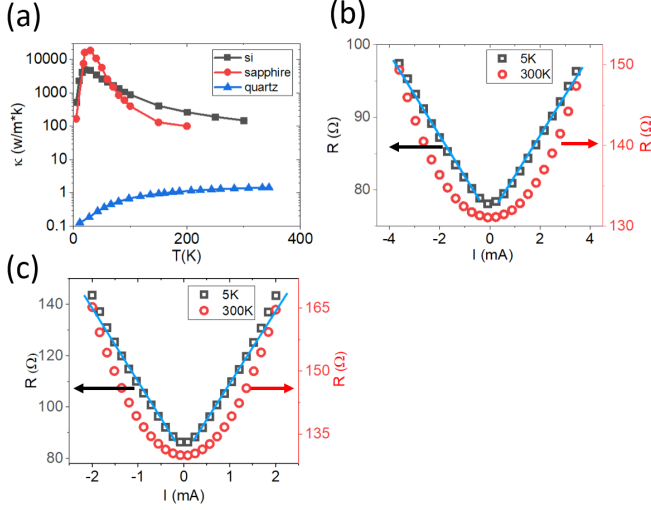


Figure 5. (a) Temperature dependence of thermal conductivity of Si, sapphire, and quartz, as labeled [from Refs. [30–32]]. (b) R vs I for a $1\mu\text{m}$ -long, 500 nm-wide Pt(5) wire fabricated on sapphire substrate, at $T = 5$ K and 300 K, as labeled. (c) Same as (b), but using a Si substrate with a 300 nm-thick thermal SiO₂ surface layer. Blue straight lines are guides for the eye.

To verify that the anomalous R vs I dependence associated with nonequilibrium current-driven phonon distribution is not limited to Pt wires on Si substrates discussed in the main text, we have studied thin-film Pt wires fabricated on sapphire and oxidized Si [surface SiO₂ thickness 300 nm]. Figure 5(a) shows the temperature-dependent thermal conductivities of Si, sapphire, and quartz. The thermal conductivity of amorphous SiO₂ on oxidized Si substrates is expected to be smaller than that of crystalline SiO₂ quartz. Regardless, these data indicate that phonon dissipation for oxidized Si is significantly less efficient than for the bare Si and for sapphire.

The R vs I dependences are shown in Figs. 5(b) and (c) for Pt(5) wires fabricated on sapphire and SiO₂, respectively. The resistivity of Pt(5) on sapphire is slightly smaller than for Pt(5) on SiO₂, and about three times smaller than for Si substrate. These differences were reproducible among different samples. The value of ρ for the sapphire substrate is slightly smaller than for SiO₂, because Pt grows on sapphire preferentially with (111) texture, as was verified by x-ray diffractometry, resulting in less electron scattering at the crystalline grain boundaries. The resistivities of thick Pt films deposited on Si approach those of Pt deposited on SiO₂, confirming the interfacial origin of the additional contribution to the resistivity of Pt on Si. We attribute this contribution to the strong electron scattering on platinum silicide formed at the Pt/Si interface.

For sapphire, the resistance increase between $I = 0$

and $I = 4$ mA is about 20 Ω both at 5 K and 300 K, Fig. 5(b). In contrast, the increase for the oxidized Si substrate is significantly larger, almost 60 Ω at 5 K, and 35 Ω at 300 K, Fig. 5(b). These results qualitatively agree with the differences between the thermal conductivities of the two substrates, which are expected to determine the phonon relaxation rates in the Pt wires. In particular, not only is the thermal conductivity of SiO₂ smaller than that of sapphire, resulting in a larger resistance increase, but it also decreases at low temperatures, in contrast to the increase in sapphire. This is consistent with the increasing current-dependent resistance variation for Pt on Si with decreasing temperature.

Despite significant quantitative differences among different substrates, at 5 K the curves $R(I)$ are almost linear both for sapphire and SiO₂, consistent with the non-equilibrium current-induced phonon distribution. A slight upcurving, more significant for SiO₂, is indicative of partial phonon thermalization, which is consistent with the longer phonon escape times in these samples than in Pt on Si, as expected from the differences among the thermal conductivities at cryogenic temperatures [Fig. 5(a)].

DEPENDENCE OF RESISTANCE ON CURRENT IN A RESISTIVE NANOCONTACT

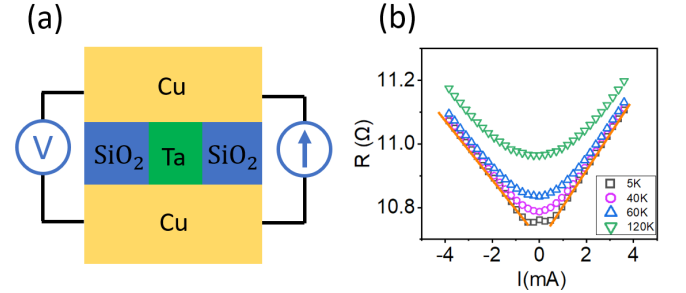


Figure 6. (a) Schematic of the resistive nanocontact, based on a 70-nm Ta(10) disk sandwiched between two thick conducting electrodes, and the pseudo-four-probe measurement setup. (b) R vs I for the studied nanocontact, at the labeled values of temperature. The straight lines are guides for the eye.

Our results for thin-film metallic wires on thermally conductive substrates suggest that nonequilibrium phonon distribution is generally formed in current-driven nanostructures characterized by efficient phonon relaxation. This hypothesis is supported by measurements of R vs I for a resistive nanocontact - a nanostructure whose geometry and thermal dissipation mechanisms completely different from those of thin-film wires. The studied nanocontact is shown schematically in Fig. 6(a). It consists of a circular Ta(10) disk with a 70 nm diameter, sandwiched between a micrometer-scale Cu(50) bottom lead, and Cu(100) top lead. The electrical leads

are separated by a $\text{SiO}_2(15)$ insulating layer. The nanostructure was fabricated using a multi-step e-beam lithography process we developed for the studies of current-induced magnetization dynamics in magnetic nanostructures, and described in detail in multiple publications [29]. The resistance of the nanocontact is measured in the pseudo-four-probe geometry, with current and voltage contacts attached to the opposite sides of the Cu leads, as shown in the schematic.

Because of the high resistivity of Ta (about $1500 \text{ n}\Omega\cdot\text{m}$ vs less than $20 \text{ n}\Omega\cdot\text{m}$ for Cu at 5 K, as determined by separate resistivity measurements), the resistance of the studied nanocontacts is dominated by the Ta(10) layer, which is also expected to provide a dominant contribution to the current-induced phonon generation. On the other hand, the thick highly conductive Cu leads provide efficient thermal dissipation. According to our analysis, if the escape of phonons from the Ta layer into the Cu leads is faster than their thermalization, a piecewise-linear dependence of resistance on current is expected. Indeed, a linear dependence $R(I)$ is observed for the studied nanocontact at $T=5 \text{ K}$ [Fig. 6(a)]. The linear dependence becomes increasingly smeared out at higher temperatures, consistent with the thermal broadening mechanisms discussed for thin-film wires in the main text.

COMSOL SIMULATION OF JOULE HEATING

To eliminate the possibility that the dependence of Pt wire resistance on current, observed in our experiments at cryogenic temperatures, can be explained by Joule heating, we performed simulations of current-dependent temperature distribution in Pt wires utilizing the COMSOL Multiphysics software. To reproduce $R(I)$ measured in experiment at 300 K, we introduce boundary thermal conductivity $1 \times 10^8 \text{ K} \cdot \text{m}^2/\text{W}$ at the interface between sample and substrate, which accounts for roughness induced imperfect thermal contact and the effects of acoustic mismatch on thermal conductivity discussed below. We note that the COMSOL simulation is based on quasi-equilibrium (thermalized) approximation for the phonon distribution underlying the Joules heating law, and diffusive approximation for the heat flow underlying the Fourier's equation. The simulated configuration closely matches the experimentally studied geometry, as illustrated in Fig. 7(a). The temperature distribution calculated at current $I = 4 \text{ mA}$ is shown in Fig. 7(b). The highest calculated temperature, near the center of the wire, is 90 K at this current. Based on the measured $R(T)$ dependence, the sample resistance is expected to increase by less than 13Ω at $I = 4 \text{ mA}$, which is inconsistent with the increase of 40Ω observed in the experiment.

Figure. 7(c) shows the calculated dependence of the average temperature in the Pt wire on current. This de-

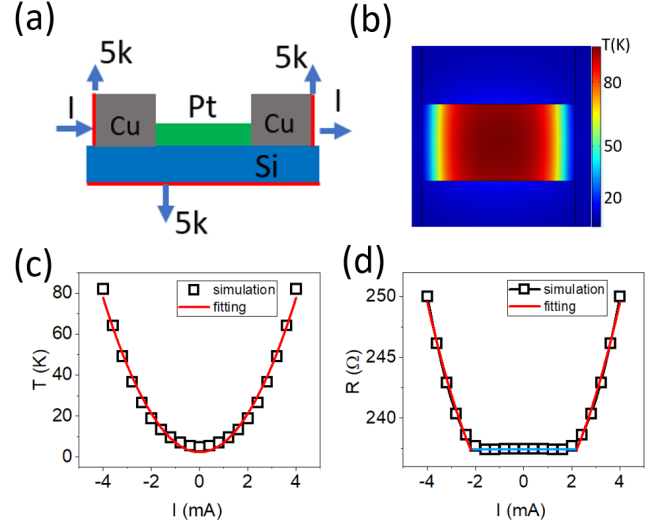


Figure 7. COMSOL simulations of Joule heating at temperature $T = 5 \text{ K}$. (a) Schematic of sample configuration used in the simulation. The simulated dimensions of the Pt wire are $1\mu\text{m} \times 500 \text{ nm} \times 5 \text{ nm}$. (b) Pseudocolor map of the calculated temperature distribution, at current $I = 4 \text{ mA}$. (c) Average sample temperature vs current. The curve is a fitting with a quadratic function. (d) Sample resistance vs current, determined from the calculated current-dependent temperature distributions such as shown in panel (b), and the measured dependence of resistivity on temperature. Blue line is $R = 229.6 \Omega$, and the red curve is a fit of the $I > 2.2 \text{ mA}$ data with the quadratic function.

pendence is precisely fitted by a quadratic function, in agreement with the qualitative analysis in the main text. Combining the calculated current-dependent spatial distribution of temperature with the measured dependence of resistivity on temperature, we obtain the dependence of sample resistance on current expected for Joule heating. The calculated current-dependent sample resistance is constant at small bias $I < 1.8 \text{ mA}$, because resistance is almost temperature-independent at $T < 20 \text{ K}$, and is well approximated by a quadratic function at $I > 2.2 \text{ mA}$ [Fig. 7(d)]. This result is inconsistent with the experimental observation of a linear dependence of resistance on current, confirming that the Joule heating approximation is inapplicable to the studied system at cryogenic temperatures.

ESTIMATION OF PHONON ESCAPE TIME FROM THE ACOUSTIC MISMATCH

We estimate the phonon escape time from Pt into the Si substrate using quasi-ballistic phonon transport approximation, which is justified by the small thickness of the studied Pt wires. The escape time is determined by the phonon scattering at the Pt/Si interface, which can be analyzed using the theory of acoustic mismatch [33].

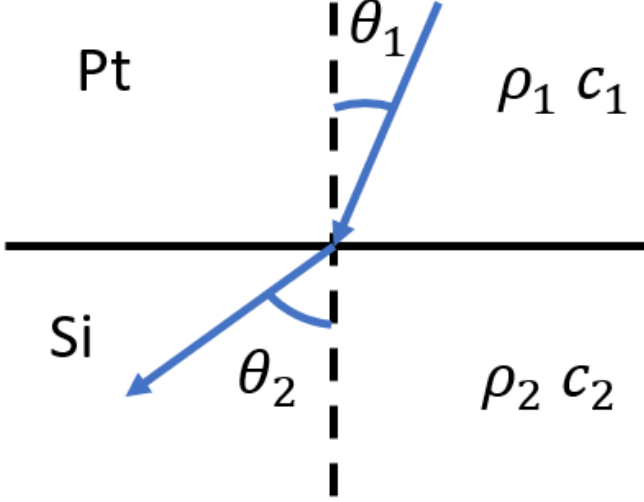


Figure 8. Schematic of the configuration used in the acoustic mismatch calculation. Phonons are generated in the Pt layer and are scattered at the Pt/Si interface. The probability of transmission into the Si substrate determines the escape rate.

For an acoustic wave incident from Pt at an angle θ_1 and refracted into Si at an angle θ_2 related to θ_1 by Snell's law [Fig. 8], the transmission coefficient is

$$\alpha = \frac{\frac{4D_2c_2}{D_1c_1} \cdot \frac{\cos\theta_2}{\cos\theta_1}}{\left(\frac{D_2c_2}{D_1c_1} + \frac{\cos\theta_2}{\cos\theta_1}\right)^2}. \quad (3)$$

Here, c is the speed of sound, and D is the mass density, with the subscript "1" used for Pt, and "2" - for Si. The escape time can be then estimated as $\tau = \frac{2d}{\alpha c_1}$. Since the speed of sound in Si is higher than in Pt, transmission is possible only at incidence angles smaller than the critical angle θ_c for the total internal reflection. The average phonon transmission coefficient is

$$\bar{\alpha} = \frac{\int_0^{\theta_c} \alpha \theta_1 d\theta_1}{\frac{\theta_c}{\frac{\pi}{2}}} = \frac{\int_0^{\theta_c} \alpha \theta_1 d\theta_1}{\frac{\pi}{2}} \quad (4)$$

For Pt(5) on Si, the average phonon escape time estimated based on Eq. (4) is $\tau_{esc} = \frac{2d}{\bar{\alpha}c_1} = 14$ ps. This estimate neglects imperfections at the Pt/Si interface that produce an acoustic barrier, which can reduce the transmission. Thus, this estimate provides a lower bound for the phonon escape time from Pt. For Au(5) on Si, similar analysis gives $\tau_{esc} = 8$ ps.

ESTIMATION OF PHONON SCATTERING TIME

Phonons generated by current do not become thermalized if the thermalizing scattering is slower than relaxation. We can estimate the phonon scattering time

based on the known phonon average mean free path, $l \approx 1 \mu\text{m}$ at 300K for Pt [34–36], and the sound velocity $c = 2.6 \times 10^3$ m/s, giving $\tau_{sc} = l_{ph}/c = 3.8 \times 10^{-10}$ s. Since not all phonon scattering is inelastic, this estimate gives a lower bound on the phonon thermalization time. Nevertheless, the estimated value of τ_{sc} is significantly larger than the estimated phonon escape time, confirming that the nonequilibrium phonon distribution generated in the studied microwires by current does not thermalize even at room temperature.

ESTIMATION OF ELECTRON-PHONON SCATTERING CROSS-SECTION

The electron-phonon scattering cross-section σ_{e-ph} determines the relationship between the population of phonons and their contribution to resistivity, as follows. According to the Matthiessen's rule for the electron mean path ($1/l_e = 1/l_{e,0} + n_{ph}\sigma_{e-ph}$). Here, $l_{e,0}$ is the mean free path in the absence of phonons, and σ_{e-ph} is understood as the average scattering cross-section over the phonon distribution. Using the Drude formula $\rho = \frac{m^*v_F}{ne^2l_e}$, we obtain

$$\rho(n_{ph}) = \rho(0) + \frac{m^*v_F n_{ph} \sigma_{e-ph}}{ne^2}, \quad (5)$$

or in the differential form

$$\sigma_{e-ph} = \frac{ne^2}{m^*v_F} \frac{d\rho}{dn_{ph}} = \frac{ne^2}{m^*v_F} \frac{\partial\rho/\partial T}{\partial n_{ph}/\partial T} \quad (6)$$

We can use Eq. (6) to extract σ_{e-ph} from the temperature dependence of resistivity and the known thermal phonon distribution. For temperatures above the Debye temperature T_D , we can approximate $n_{ph} \approx 3n_{at}T/T_D$, so that

$$\sigma_{e-ph} \approx \frac{ne^2 T_D}{3n_{at}m^*v_F} \frac{\partial\rho}{\partial T}. \quad (7)$$

We are interested in the scattering cross section on large-momentum phonons generated by current, corresponding to the linear regime of $R(I)$ observed at sufficiently large currents, as discussed in the main text. Large-momentum thermal phonons also dominate electron-phonon scattering in thermal equilibrium at high temperatures ($T > T_D$), due to the dominance of their phase volume over the small-momentum phonons. Thus, we can assume that the average scattering cross section on thermal phonons above the Debye temperature is similar to that on current-generated phonons in the linear $R(I)$ regime (at sufficiently large bias). We use the dependence $\rho(T)$ close to $T = 300$ K and Eq. (7) to obtain

$\sigma_{e-ph} = 1.8 \times 10^{-22} \text{ m}^2$ for Pt, and $\sigma_{e-ph} = 1.3 \times 10^{-22} \text{ m}^2$ for Au.

-
- [1] A. Zangwill, *Modern electrodynamics* (Cambridge University Press, 2013).
- [2] J.-P. Ansermet and S. D. Bréchet, *Principles of thermodynamics* (Cambridge University Press, 2019).
- [3] I. N. Krivorotov, N. C. Emley, A. G. F. Garcia, J. C. Sankey, S. I. Kiselev, D. C. Ralph, and R. A. Buhrman, *Phys. Rev. Lett.* **93**, 166603 (2004).
- [4] R. H. Liu, W. L. Lim, and S. Urazhdin, *Phys. Rev. Lett.* **110**, 147601 (2013).
- [5] E. Pop, S. Sinha, and K. E. Goodson, *Proceedings of the IEEE* **94**, 1587 (2006).
- [6] E. Pop, *Nano Research* **3**, 147 (2010).
- [7] A. Giri, J. T. Gaskins, B. F. Donovan, C. Szejewski, R. J. Warzoha, M. A. Rodriguez, J. Ihlefeld, and P. E. Hopkins, *Journal of Applied Physics* **117**, 105105 (2015).
- [8] S. Ono, *Physical Review B* **97**, 054310 (2018).
- [9] M. L. Roukes, M. R. Freeman, R. S. Germain, R. C. Richardson, and M. B. Ketchen, *Phys. Rev. Lett.* **55**, 422 (1985).
- [10] F. C. Wellstood, C. Urbina, and J. Clarke, *Phys. Rev. B* **49**, 5942 (1994).
- [11] A. H. Steinbach, J. M. Martinis, and M. H. Devoret, *Phys. Rev. Lett.* **76**, 3806 (1996).
- [12] S. K. Tripathy, G. Xu, X. Mu, Y. J. Ding, K. Wang, Y. Cao, D. Jena, and J. B. Khurgin, *Applied Physics Letters* **92**, 013513 (2008).
- [13] I. Klett and B. Rethfeld, *Physical Review B* **98**, 144306 (2018).
- [14] J. Kash, J. Tsang, and J. Hvam, *Physical review letters* **54**, 2151 (1985).
- [15] N. Del Fatti, C. Voisin, M. Achermann, S. Tzortzakis, D. Christofilos, and F. Vallée, *Physical Review B* **61**, 16956 (2000).
- [16] J. Li and J. E. Han, *Phys. Rev. B* **97**, 205412 (2018).
- [17] L. Siddiqui, A. W. Ghosh, and S. Datta, *Phys. Rev. B* **76**, 085433 (2007).
- [18] T. Chase, M. Trigo, A. H. Reid, R. Li, T. Vecchione, X. Shen, S. Weathersby, R. Coffee, N. Hartmann, D. A. Reis, X. J. Wang, and H. A. Durr, *Applied Physics Letters* **108**, 041909 (2016), <https://doi.org/10.1063/1.4940981>.
- [19] A. X. Gray, M. C. Hoffmann, J. Jeong, N. P. Aetukuri, D. Zhu, H. Y. Hwang, N. C. Brandt, H. Wen, A. J. Sternbach, S. Bonetti, A. H. Reid, R. Kukreja, C. Graves, T. Wang, P. Granitzka, Z. Chen, D. J. Higley, T. Chase, E. Jal, E. Abreu, M. K. Liu, T.-C. Weng, D. Sokaras, D. Nordlund, M. Chollet, R. Alonso-Mori, H. Lemke, J. M. Glowina, M. Trigo, Y. Zhu, H. Ohldag, J. W. Freeland, M. G. Samant, J. Berakdar, R. D. Averitt, K. A. Nelson, S. S. P. Parkin, and H. A. Dürr, *Phys. Rev. B* **98**, 045104 (2018).
- [20] S. Huberman, R. A. Duncan, K. Chen, B. Song, V. Chiloyan, Z. Ding, A. A. Maznev, G. Chen, and K. A. Nelson, *Science* **364**, 375 (2019), <https://science.sciencemag.org/content/364/6438/375.full.pdf>.
- [21] L. Liu, T. Moriyama, D. C. Ralph, and R. A. Buhrman, *Phys. Rev. Lett.* **106**, 036601 (2011).
- [22] T. Jungwirth, J. Wunderlich, and K. Olejník, *Nature materials* **11**, 382 (2012).
- [23] K. Ando, S. Takahashi, K. Harii, K. Sasage, J. Ieda, S. Maekawa, and E. Saitoh, *Phys. Rev. Lett.* **101**, 036601 (2008).
- [24] V. Demidov, S. Urazhdin, A. Zholud, A. Sadovnikov, and S. Demokritov, *Applied Physics Letters* **105**, 172410 (2014).
- [25] M. Yang, K. Cai, H. Ju, K. W. Edmonds, G. Yang, S. Liu, B. Li, B. Zhang, Y. Sheng, S. Wang, *et al.*, *Scientific reports* **6**, 20778 (2016).
- [26] J.-g. Kang, J.-S. Park, K.-B. Park, J. Shin, E.-A. Lee, S. Noh, and H.-J. Lee, *Micro and Nano Systems Letters* **5**, 26 (2017).
- [27] See the supplementary materials that accompany this article.
- [28] N. F. Mott and H. Jones, *The theory of the properties of metals and alloys* (Courier Corporation, 1958).
- [29] A. Zholud, R. Freeman, R. Cao, A. Srivastava, and S. Urazhdin, *Phys. Rev. Lett.* **119**, 257201 (2017).
- [30] M. Ashghi, M. Touzelbaev, K. Goodson, Y. Leung, and S. Wong, *Journal of Heat Transfer* **120**, 30 (1998).
- [31] E. R. Dobrovinskaya, L. A. Lytvynov, and V. Pishchik, *Sapphire: material, manufacturing, applications* (Springer Science & Business Media, 2009).
- [32] C. Glassbrenner and G. A. Slack, *Physical Review* **134**, A1058 (1964).
- [33] W. Little, *Canadian Journal of Physics* **37**, 334 (1959).
- [34] K. T. Regner, D. P. Sellan, Z. Su, C. H. Amon, A. J. McGaughey, and J. A. Malen, *Nature communications* **4**, 1640 (2013).
- [35] O. Bourgeois, D. Tainoff, A. Tavakoli, Y. Liu, C. Blanc, M. Boukhari, A. Barski, and E. Hadji, *Comptes Rendus Physique* **17**, 1154 (2016).
- [36] Y. Hu, L. Zeng, A. J. Minnich, M. S. Dresselhaus, and G. Chen, *Nature nanotechnology* **10**, 701 (2015).